IEICE TRANSACTIONS

on Electronics

DOI:10.1587/transele.2023ECP5060

Publicized:2024/05/21

A PUBLICATION OF THE ELECTRONICS SOCIETY

The Institute of Electronics, Information and Communication Engineers
Kikai-Shinko-Kaikan Bldg., 5-8, Shibakoen 3chome, Minato-ku, TOKYO, 105-0011 JAPAN

PAPER

High-Precision Temperature Analysis Considering Temperature-Dependent Tissue Properties in Renal Denervation

Tohgo HOSODA[†], ***Student Member and*** **Kazuyuki SAITO**[††], ***Member***

SUMMARY Transcatheter renal denervation (RDN) is a treatment for resistant hypertension, which is performed by ablating the renal nerves located outside the artery using a catheter from inside the artery. Our previous studies simulated the temperature during RDN by using constant physical properties of biological tissue to validate the various catheter RDN devices. Some other studies report temperature dependence of physical properties of biological tissues. However, there are no studies that have measured the electrical properties of low water content tissues. Adipose tissue, a type of low water content tissue, is related to RDN closely. Therefore, it is important to know the temperature dependence of the electrical constants of adipose tissue. In this study, we measured the relationship between the electrical constants and the temperature of bovine adipose tissue. Next, the obtained equation of the relationship between relative permittivity of adipose tissue and temperature was introduced. In addition, the temperature dependence of the electrical constants of high water content tissues and the temperature dependence of the thermal constants of biological tissues were also introduced into the temperature analysis. After 180 seconds of heating, the temperature of the model with the temperature dependence of the physical properties was 7.25 °C lower than the model without the temperature dependence of the physical properties at a certain position. From the results, it can be said that the temperature dependence of physical properties will be significant when an accurate temperature analysis is required.

key words: *Renal denervation, temperature-dependent tissue properties, human body model, biological tissue, finite-difference time-domain (FDTD) method, temperature analysis*

1. Introduction

In recent years, hypertension has become a common disease worldwide. It is estimated that approximately 31.1% of the adult population is currently affected [1] and the number of patients is still increasing [2]. One type of hypertension is resistant hypertension, a disease in which hypertension does not decrease to the target hypertension level even with the use of three or more anti-hypertensive drugs. It is estimated that approximately 10.1% of patients treated for hypertension have resistant hypertension [1].

Transcatheter Renal Denervation (RDN) is being investigated as a new treatment method for resistant hypertension [3]. Figure 1 shows an overview of the RDN treatment. The RDN is conducted by inserting a catheter into the renal artery and ablating the nerve outside the artery by heating it to over 60 °C, thereby producing anti-hypotensive effects. Although RDN is promising as a powerful and minimally invasive treatment method, temperature monitoring of the heated area is difficult. Because the operation is usually performed blindly, and it cannot be confirmed whether the nerves have. Thus, some reports show no significant effect on blood pressure reduction at 6 months postoperatively [4]–[6]. Another factor that contributes to the lack of antihypertensive effect is the use of previously designed, RF-based devices for heating. Rakhmadi *et al.* found that microwave-based devices were able to ablate regions further away from the renal artery than RF-based devices [7]. Microwave catheter RDNs seem to be more effective, therefore we need to know more about treatment in microwave catheter-based devices. Hence, we propose the high-precision temperature analysis using microwave RDN device.

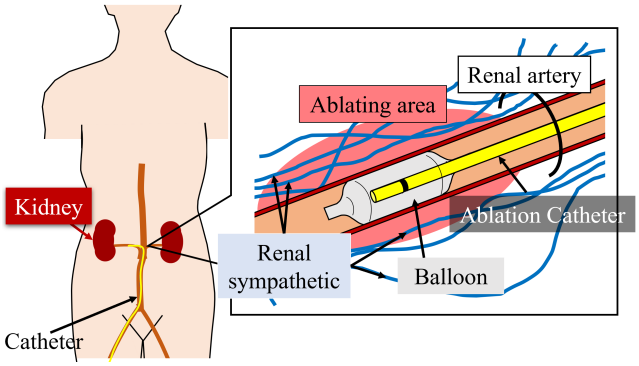

Fig. 1 Overview of catheter RDN system.

The area around blood vessels, where the treatment site for RDN, is surrounded by adipose tissue. According to [8] and [9], there are reports of temperature dependence of electrical and thermal constants and blood flow rate in biological tissues. In particular, many papers have reported on easily accessible tissues such as porcine liver [10]–[15]. However, in the authors' investigation, the temperature dependence of electrical constants of low water content tissues such as adipose tissue has not been investigated. This paper aims to clarify the high-precision temperature distributions during the RDN treatment considering the temperature dependence physical properties of biological tissue and blood flow rate for every tissue close to the renal artery. For this purpose, we first measured and clarified the temperature dependence of the electrical constants of low water content tissues, which had not been clarified. Then, based on several studies [10]–[13], [16]–[24], we formulated our own relationship between electrical and thermal constants of physical prop-

[†]Graduate School of Science and Engineering, Chiba University, 1-33 Yayoi-cho, Inage-ku, Chiba 263-8522, Japan.

[††]Center for Frontier Medical Engineering, Chiba University, 1-33 Yayoi-cho, Inage-ku, Chiba 263-8522, Japan.

erties and temperature and blood flow rate. Furthermore, numerical analyses were performed using temperature dependence physical properties formulated to the human body model TARO [25].

2. Preparation for temperature calculations

2.1 Analytical procedure

Figure 2 shows the flowchart for electromagnetic and temperature analysis. First, electromagnetic field analysis is carried out using the finite-difference time-domain (FDTD) method [26] to calculate the electromagnetic field distribution in the analytical model. Then, the Specific Absorption Rate (SAR) [28] is calculated from the electromagnetic field distribution using the following equation:

$$\mathrm{SAR} = \frac{\sigma}{\rho} E^2 \qquad [\mathrm{W/kg}] \tag{1}$$

where σ is the electrical conductivity of the biological tissue [S/m], ρ is the density of the tissue [kg/m^3], and E is the root-mean-square electrical field [V/m].

Following the calculation of SAR, the temperature distribution is calculated by solving the bioheat transfer equation [27]:

$$\rho c \frac{\partial T}{\partial t} = \kappa \nabla^2 T - c_b W_b (T - T_b) + \rho \cdot \mathrm{SAR} \tag{2}$$

where ρ is the density [kg/m^3], c is the specific heat capacity at constant pressure [J/kg $\cdot$ K], T is temperature [K], t is time [s], k is thermal conductivity [W/m $\cdot$ K], c_b is the specific heat of blood [J/kg $\cdot$ K], W_b is blood flow rate [kg/m^3 $\cdot$ s], T_b is the temperature of blood circulating in tissue [K].

The first and second terms on the right-hand side of Eq. (2) describe the heat transport in each tissue and between tissue and blood, respectively. The tissue heating due to the absorption of an electric field is shown in the third term of Eq. (2). The temperature distribution is then calculated by solving Eq. (2) by FDTD according to [28]. In this study, the physical properties of the tissue were updated every 1.0 s. Because of the significant change in blood flow rate up to 50 °C, the physical properties of tissue were updated every 1 °C from 37 °C to 50 °C and every 5 °C from 50 °C to 100 °C. These numerical calculations were performed by self-written codes.

2.2 Measurement of electrical properties for low water content tissues

In the RDN treatment, the renal artery into which the catheter is inserted is surrounded by adipose tissue, one of the low water content tissues. The previous study clarified the temperature dependence of adipose tissue in the MHz band [29]. However, the temperature dependence of the electrical constants of adipose tissue at 2.45 GHz was not yet clarified.

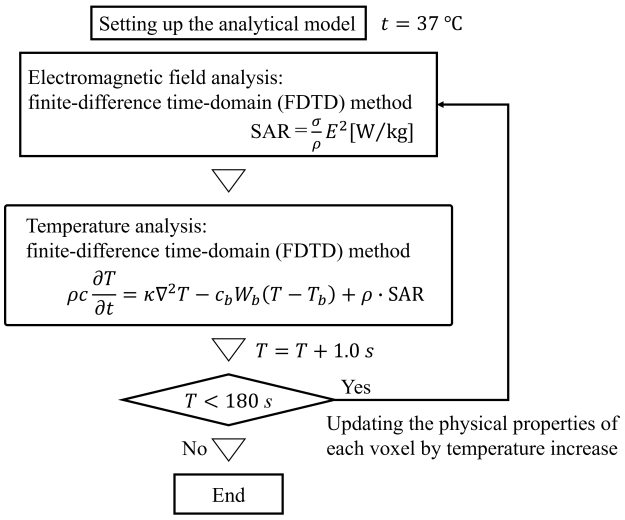

Fig. 2 Calculation procedure.

By the way, in the field of biological electromagnetic compatibility, adipose tissue is conventionally analyzed without classification of brown and white adipose tissue [31]. The "Database of Tissue Dielectric Properties for Electromagnetic Modeling of Human Body" provided by the National Institute of Information and Communications Technology (NICT) is not classified as well. Therefore, the temperature dependence of the electrical constants at 2.45 GHz was clarified by measuring the electrical constants of 22 available bovine adipose samples without the classification.

A slim form probe of a Keysight 85070E Dielectric Probe Kit (Keysight Technologies, Santa Rosa, CA, USA) was employed for this purpose. In this measurement, the tissue was heated in a water bath for 10 minutes, and the tissue surface was quickly measured after removal from the water bath in order to confirm the temperature dependence of electrical constants. The temperature in the hot water bath was then changed and the tissue was reheated after the water temperature was updated. The temperature in the water bath was changed to 40, 60, 80 and 100 °C. Each adipose tissue sample was kept in a separate zip sealed bag to prevent tissue hydration, and the measurement section of tissue was lightly wiped before measurement. In order to reduce measurement error due to the measurement section, measurements were conducted in the same position by marking the tissue surface.

Figure 3 shows the relationship between the relative permittivity and electrical conductivity of bovine adipose tissue and the surface temperature of tissues, obtained by excluding more than three times the standard deviation from the mean of the measurement results. Both the relative permittivity and electrical conductivity show a large spread. In order to characterise various low water content tissues, the approximate curves of relative permittivity is obtained from Fig. 3. The function based on the approximate curves obtained are shown as follows:

$$\varepsilon_{r\,\mathrm{adipose}}(T) = -0.0003T^2 + 0.0207T + 4.6367 + C_{\varepsilon_r} \tag{3}$$

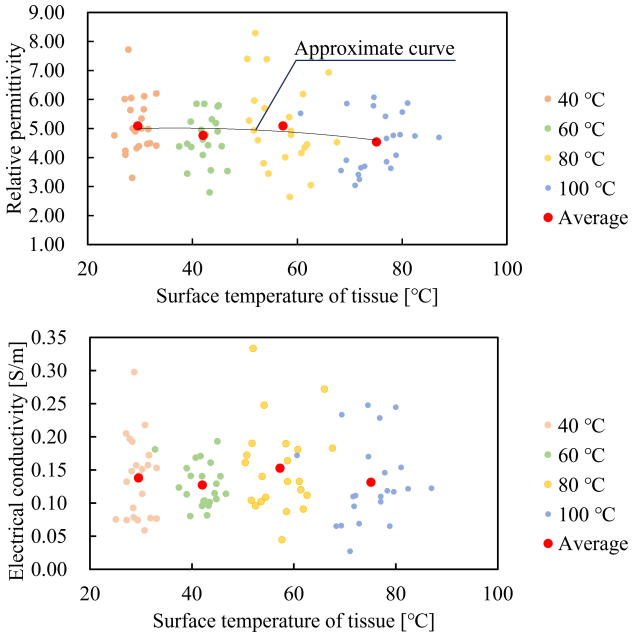

Fig. 3 Temperature dependence of relative permittivity and electrical conductivity of bovine adipose tissue.

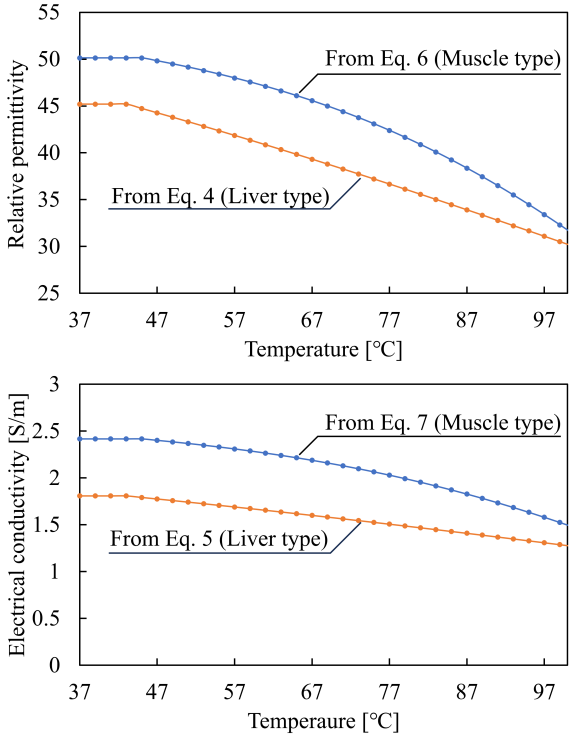

Fig. 4 Temperature dependence of the relative permittivity and electrical conductivity of high water content tissues.

On the other hand, the electrical conductivity showed a larger coefficient of variation. In particular, a comparison of the dispersion coefficients of relative permittivity and electrical conductivity per heating temperature showed that the dispersion coefficient of electrical conductivity was twice as large as that of relative permittivity. Therefore, the temperature dependence of electrical conductivity could not be determined. Consequently, the electrical conductivity of adipose tissue was assumed to be independent of temperature. We assumed that low water content tissue would have a similar changing rate to adipose tissue in the temperature dependence of the electrical constants. Therefore, C_{ε_r} of Eq. (3) was set in order to make Eq. (3) at $T = 37$ °C the same as the relative permittivity of organs and tissues at 2.45 GHz [31]. For example, the relative permittivity of human adipose tissue at 2.45 GHz is 10.8 [31], so C_{ε_r} of Eq. (3) was set to 5.81.

2.3 Temperature dependence of the electrical properties of high water content tissues

In [8], [10], the temperature dependence of relative permittivity and electrical conductivity were measured in various high water content tissues. We characterised the temperature dependence of the electrical constants of high water content tissues by the method of Endo *et al.* [10]. Figure 4 shows the relationship between electrical constants and temperature in porcine liver [10] and muscle which is measured using the same method as Endo *et al* [10] .

Even in high water content tissues, different types of tissue have different changing rate in the temperature dependence of the electrical constants. Consequently, we have classified high water content tissues into two types: ⟨ Liver type ⟩ based on the liver: $\varepsilon_r(T = 37) \leq 45$, and ⟨ Muscle type ⟩ based on the muscle: $45 < \varepsilon_r(T = 37)$, and formulated by classification as below:

$$\varepsilon_{r\,\mathrm{liver}}(T) = 69.58 \times 0.0006^{\exp(-0.0379\times(-0.298T+86.0))} + 1.42 + C_{\varepsilon_r} \quad (4)$$

$$\sigma_{\mathrm{liver}}(T) = 2.8 \times 0.0044^{\exp(-0.0344\times(-0.298T+86.0))} + C_{\sigma} \quad (5)$$

$$\varepsilon_{r\,\mathrm{muscle}}(T) = 53 \times 10^{-31\times\exp(-0.09\times(-0.367T+90.399))} + 1.83 + C_{\varepsilon_r} \quad (6)$$

$$\sigma_{\mathrm{muscle}}(T) = 2.8 \times 10^{-31\times\exp(-0.09\times(-0.367T+90.399))} + C_{\sigma} \quad (7)$$

Equations (4) and (5) are the functions of liver type, and Eqs. (6) and (7) are the functions of muscle type. We determined C_{ε_r} and C_{σ} in the same way as the low water content tissues, respectively. For example, the relative permittivity and electrical conductivity of the blood vessel wall at 2.45 GHz are 42.5 and 1.44 [31], respectively, so C_{ε_r} and C_{σ} of Eqs. (4) and (5) were set to -2.62 and -0.36, respectively. Furthermore, the relative permittivity and electrical conductivity of the stomach at 2.45 GHz are 62.2 and 2.11 [31], respectively, so C_{ε_r} and C_{σ} of Eqs. (6) and (7) were set to 12.07 and -0.21, respectively. Figure 5 shows the temperature dependence of the relative permittivity and electrical conductivity of biological tissues used in this study. These figures are plotted according to Eqs. (3) to (7). The positions

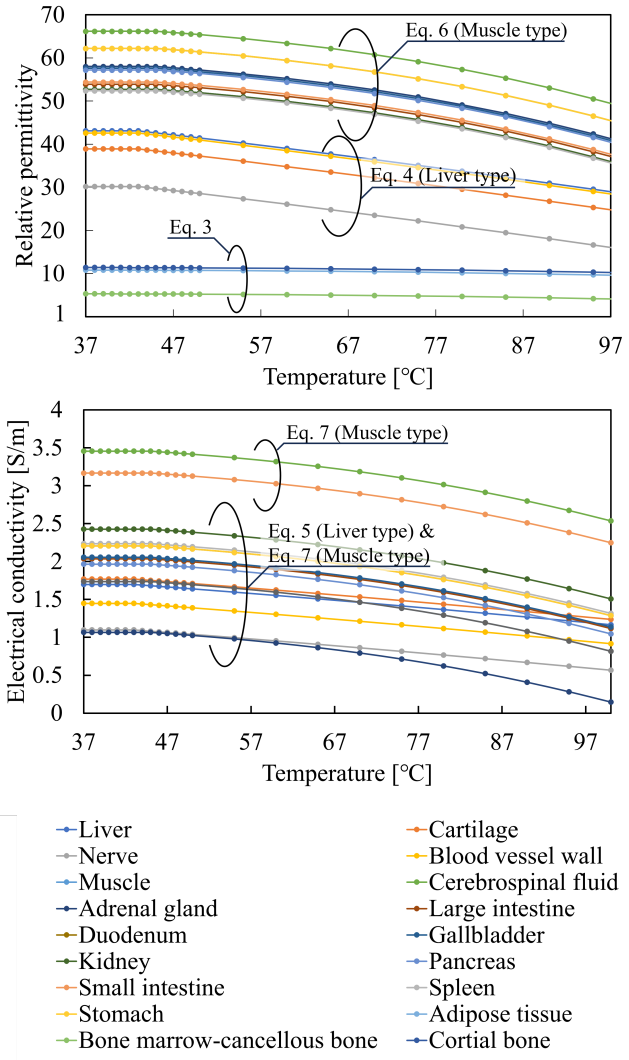

Fig. 5 Temperature dependence of relative permittivity and electrical conductivity of biological tissues in the analytical model.

of the dots are the values actually used in the update of the electrical constants of biological tissues.

2.4 Temperature dependence of the thermal properties of biological tissues

According to [13], the physical properties of biological tissues $(\varepsilon_r, \sigma, k, c)$ are highly dependent on water content. Therefore, for convenience, specific heat and thermal conductivity were also classified by the ε_r of each biological tissue. The specific heat was classified into three types and the thermal conductivity into four types.

The temperature dependence of specific heat and thermal conductivity has already been shown by some studies [11]–[13], [16]–[20], [23], [24]. Figure 6 shows typical measured results of the temperature dependence of specific heat and an approximate curve obtained from the measured results [11], [13], [20], [23]. All measurements were performed using the Differential Scanning Calorimetry (DSC) method.

As shown below, in specific heat, we have classified biological tissues into three types: ⟨ Gray matter type ⟩ based on gray matter: $45 < \varepsilon_r(T = 37)$, ⟨ Liver type ⟩ based on liver: $20 < \varepsilon_r(T = 37) \leq 45$, and ⟨ Adipose tissue type ⟩ based on adipose tissue: $\varepsilon_r(T = 37) \leq 20$, and formulated by classification as below:

$$c_{\text{gray matter}}(T) = 3449.4 \cdot \exp(0.00012T) + C_c \quad (8)$$

$$c_{\text{liver}}(T) = 3279 \cdot \exp(0.0014T) + C_c \quad (9)$$

$$c_{\text{adipose}}(T) = 2118.3 \cdot \exp(0.0022T) + C_c \quad (10)$$

Equations (8), (9) and (10) are an exponential approximation for gray matter type derived from [23], liver type derived from [11], [13] and adipose tissue type derived from [20], respectively. We determined C_c in the same way as the electrical constants of biological tissues. For example, specific heat of stomach, blood vessel wall, and cortial bone at 2.45 GHz are 3690, 3306, and 1313, respectively [31], so C_c of Eqs. (8), (9) and (10) were set to 84, -147 and -984, respectively.

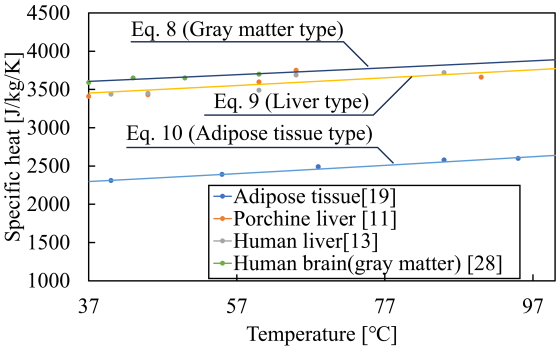

Fig. 6 Temperature dependence of specific heat.

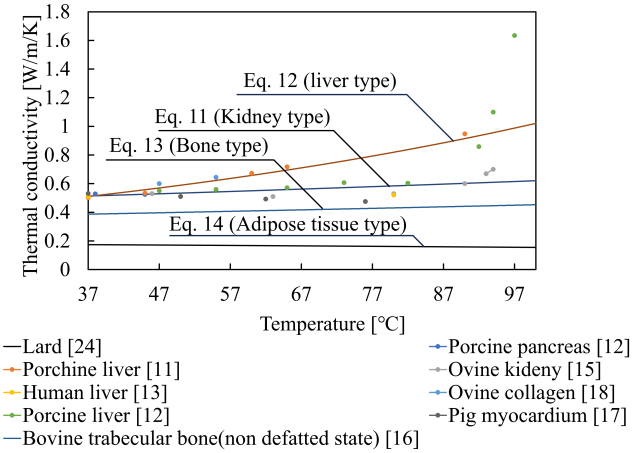

Fig. 7 Temperature dependence of thermal conductivity.

Figure 7 shows typical measurements of thermal conductivity and temperature dependence, the approximate

curves obtained from the reference to the measurements, and their functions [11]–[13], [16]–[19], [24].

As shown below, in thermal conductivity, we have classified biological tissues into four types: ⟨ Kidney type ⟩ based on kidney: $50 < \varepsilon_r(T = 37)$, ⟨ Liver type ⟩ based on liver: $20 < \varepsilon_r(T = 37) \leq 50$, ⟨ Bone type ⟩ based on bone: $\varepsilon_r(T = 37) \leq 20$, and ⟨ Adipose tissue type ⟩ based on adipose tissue: $\varepsilon_r(T = 37) = 10.8$ [31] and formulated by classification as below:

$$k_{\text{kidney}}(T) = 0.46 \cdot \exp(0.003T) + C_k \tag{11}$$

$$k_{\text{liver}}(T) = 0.3402 \cdot \exp(0.011T) + C_k \tag{12}$$

$$k_{\text{bone}}(T) = 0.3526 \cdot \exp(0.0025T) + C_k \tag{13}$$

$$k_{\text{adipose}}(T) = 0.1822 - 2.0565 \times 10^{-4}T - 7.3267 \times 10^{-7}T^2 + 0.004 \tag{14}$$

Equations (11), (12), (13), and (14) are functions for Kidney type, based on [19], liver type based on [11]–[13], bone type based on [16] and Adipose tissue type from [24], respectively. We determined C_k in the same way as the electrical constants. For example, thermal conductivity of stomach, blood vessel wall, and cortial bone at 2.45 GHz are 0.53, 0.46, and 0.32, respectively [31], so C_k of Eqs. (11), (12) and (13) were set to 0.02, 0.01 and -0.06, respectively.

Figure 8 shows the temperature dependence on the specific heats and thermal conductivities of biological tissues used in our study. These figures are plotted according to Eqs. (8) to (14). As in Fig. 5, the positions of the dots are the values actually used in the updating of the thermal constants of biological tissues.

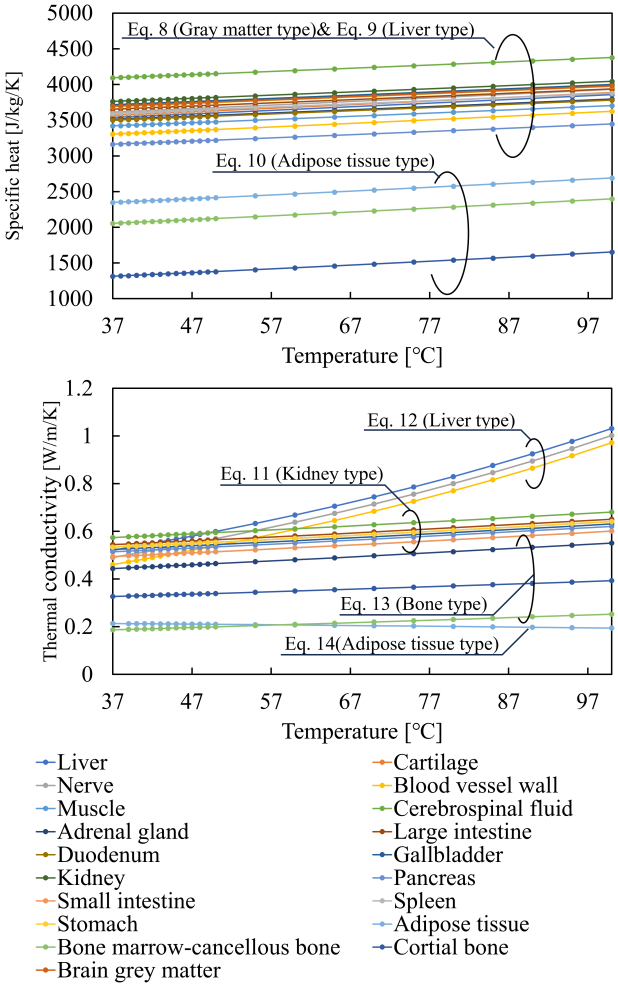

Fig. 8 Temperature dependence of specific heat and thermal conductivity of biological tissues in the analytical model.

2.5 Temperature dependence of blood flow rate

Blood perfusion has an impact on heat diffusion and temperature distribution inside biological tissues. Hence, their possible variation as a function of temperature could in turn influence the final therapeutic outcome of thermal treatments [30]. For high-precision temperature analysis, the temperature dependence of the blood flow rate must be considered. In this study, the blood flow rates shown below were followed [21].

$$W_b(T) = W_{b(T=37)} \cdot \left(1 + 7\exp\left(\frac{-(T-45)^2}{12}\right)\right) \tag{15}$$

$$W_b(T) = W_{b(T=37)} \cdot \left(1 + \exp\left(\frac{-(T-45)^2}{12}\right)\right) \tag{16}$$

Equations (15) and (16) indicate the temperature dependence of blood flow rate for organs and for adipose tissue, respectively. In this study, the blood flow rates of the target organs obtained from [31] were used as the initial term at 37 °C to express the blood flow rate in various organs. Figure 9 shows the blood flow rates used in this study. For the contents of the small intestine, where no blood flows, and for tissues such as cerebral spinal fluid, we set the blood flow rate as 0 regardless of temperature.

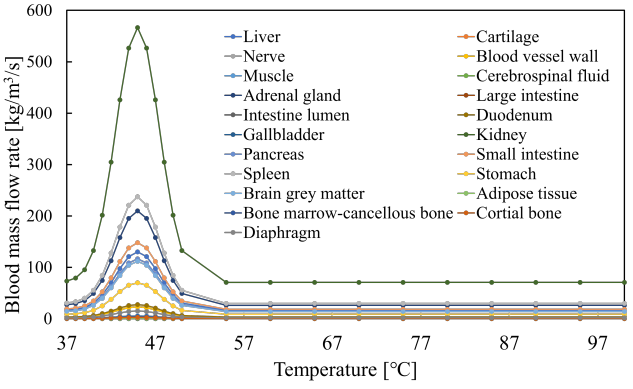

Fig. 9 Temperature dependence of blood flow rates in the tissues used in the analytical model.

Table 1 Analytical conditions.

For Electromagnetic analyses	
Minimum cell size [mm]	0.5
Maximum cell size [mm]	0.1
Time step[s]	2.33×10^{-13}
Absorbing boundary condition	Mur (1st order)
For Temperature analyses	
Minimum cell size [mm]	0.5
Maximum cell size [mm]	0.1
Time step[s]	0.001
Boundary temperature [°C]	37.0
Initial temperature [°C]	37.0

3. Numerical model

The analytical model is shown in Fig. 10 (a). In this study, the model was created by cutting out the area including the renal nerve, which is the treatment site for RDN, from the human model TARO and processing it in the same way as in previous studies [33]. A blood vessel model with an inner diameter of 6 mm and an outer diameter of 7 mm was designed at the center, and a catheter was inserted into the central axis of the blood vessel. A schematic diagram of the inserted catheter is shown in Fig. 10 (b) [33]. The microwave catheter consisted of a flexible coaxial-slot antenna and a balloon. The outer diameter of the balloon is the same as the inner diameter of the blood vessel. We add a flexible coaxial antenna with single-slot, and a short circuit between the inner and outer tip. The width of a ring slot is 1 mm located 10 mm from the tip. The feeding point was located at the other end from the ring slot. The inside of the balloon was filled with water fixed at 37 °C to have a cooling effect on the blood vessel surface.

In this analysis, nonuniform grids were used and small cells were used only around the vessels. Table 1 shows the analytical conditions of the calculation. The input power, operating frequency, and heating time of the antenna were set to 45 W, 2.45 GHz and 180 s, respectively. The same voxels were used for the electromagnetic and temperature analyses.

In this study, four points sites were used as observation points for the temperature transition, as shown in Fig. 10 (a). “A” was the observation point inside the vessel wall in touch with the small intestine (x = 3 mm, y = 0), and “B” was the observation point inside the small intestine (x = 6 mm, y = 0), 3 mm away from “A”. Similarly, “C” was the observation point inside the vessel wall (x = -3 mm, y = 0) in touch with the adipose tissue, and “D” was the observation point inside the adipose tissue (x = -6 mm, y = 0). Numerical analysis was conducted under the following two different conditions: Model 1: with the temperature dependence of the electrical and thermal constants and variable blood flow rate, and Model 2: all physical properties are constant (independent of temperature). The physical properties of the organs in Model 2 obtained from [31] were used.

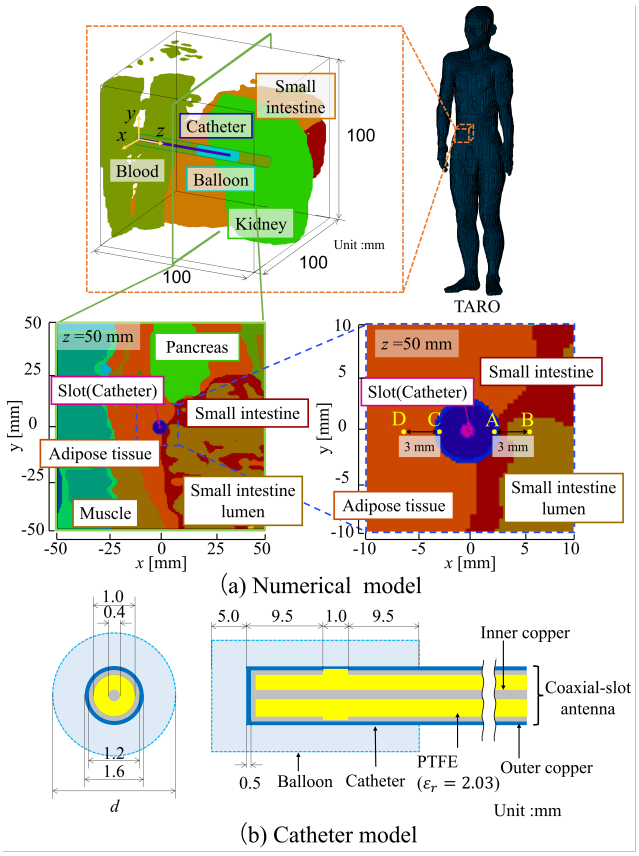

Fig. 10 Numerical model,

4. Results

Figure 11 shows the temperature distributions after 180 s of heating. Figure 11 is the same cross-section as that in Fig. 10 (a), sliced at z = 50 mm. In both cases, specific heating regions were observed near the small intestine (x = 5 mm, y = -5 mm), while a relatively low temperature distribution was observed on the adipose tissue side (x = -10 mm, y = 0 mm). The heating area on the small intestine side (x = 5 mm, y = 5 mm) was narrower in Model 1 than in Model 2. On the other hand, near the adipose tissue side (x = -10 mm, y = 0 mm), there was no significant difference in the size of the heated area between Model 1 and Model 2. Although the blood vessel surface is the biological tissue closest to the catheter, the water temperature inside the balloon was kept at a fixed temperature of 37 °C, resulting in a reduced temperature rise. The results of the temperature transition at points “A” to “D” are shown in Fig. 12. The temperature at “A”, the temperature observation point on the surface of the vessel, was maintained at a temperature difference of approximately 1.25 °C between Model 1 and Model 2 after 5 s from the start of heating. The temperature at “C” was almost the same whether the temperature dependence of physical properties considered or not.

The temperature difference between Model 1 and Model 2 at “B”, located 3 mm away from “A” towards the small

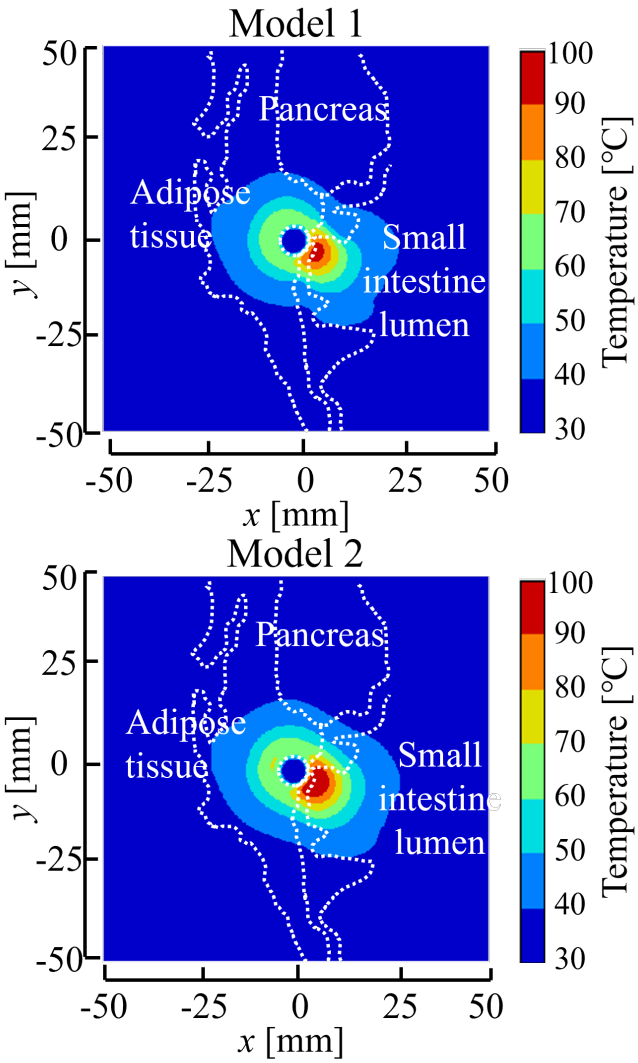

Fig. 11 Temperature distribution after 180 s heating.

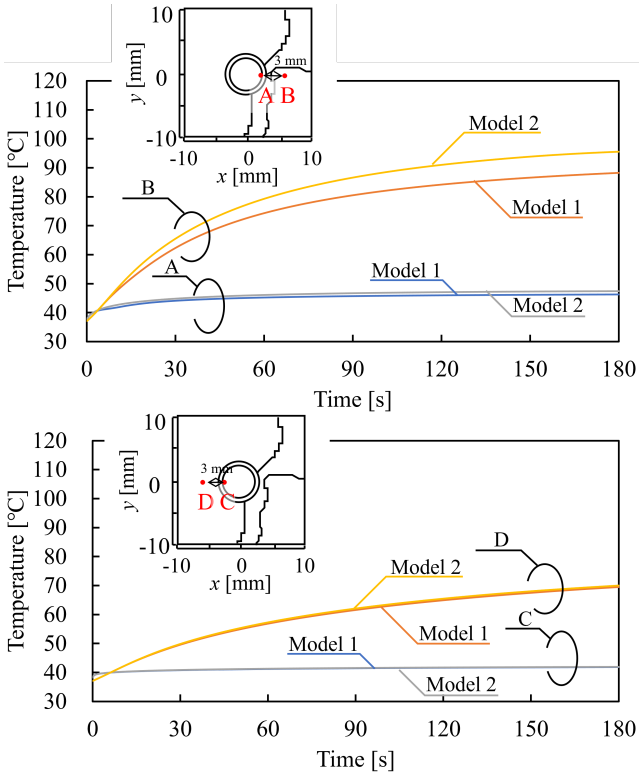

Fig. 12 Temperature transition.

intestine, increased from the start of heating. Then, the temperature difference between Model 1 and Model 2 after 180 s from the start of heating was 7.25 °C. On the other hand, the temperature difference between Model 1 and Model 2 at "D", located 3 mm away from "C" towards the adipose tissue, was kept almost the same from the start of heating. The temperature difference between Model 1 and Model 2 after 180 s from the start of heating at "D" was 0.54 °C. This result indicates that the changes were smaller than on the small intestine side. Since these results vary the physical properties, we are not sure which parameter has the greatest influence.

Model 1 required approximately 36 times longer calculation times than Model 2. Though the temperature analysis performs the same amount of calculation with and without updating the physical properties of biological tissue, electromagnetic field analysis was performed each time the physical properties of biological tissues were updated.

5. Conclusion

In this study, the relative permittivity of low water content tissues, which have yet to be clarified, were measured in order to perform a more realistic analysis. As a result, there was a large spread in the measured values of both relative permittivity and electrical conductivity. Although the temperature dependence of the relative permittivity was determined, the temperature dependence of the conductivity could not be determined. Moreover, a high-precision temperature analysis considering the temperature dependence of the physical properties and blood flow rates was performed on the human body model TARO. The results of the temperature analyses showed that considering the temperature dependence produced a maximum temperature difference of up to 7.25 °C when compared to the model without the temperature dependences. However, the shape of the temperature distribution showed a minor change compared to Model 1 and Model 2, in our case. Incidentally, when the analysis is performed under the condition that the physical properties of the biological tissue were updated for every 1 s temperature analysis, i.e., when the physical properties of the biological tissue were updated 180 times, the computation time takes approximately 36 times longer. In the future, the computational speed may be resolved, making the process more practical. Finally, our study will be useful for future RDN applicator development.

Acknowledgments

The authors would like to thank Takuma Hattori, the Faculty of Engineering, Chiba University, Chiba, Japan, for his assistance with the experiments.

References

[1] K. T. Mills, J. D. Bundy, T. N. Kelly, J. E. Reed, P. M. Kearney, K. Reynolds, J. Chen, and J. He, "Global disparities of hypertension prevalence and control: A systematic analysis of population-based studies from 90 countries," Circulation, vol. 134, no. 6, pp. 441-450, 2016.

[2] H. Salem, D. Hasan, A. Eameash, H. A. Elawady, S. Hasan, and R. Ali, "Worldwide prevalence of hypertension: A pooled meta-analysis of 1670 studies in 71 countries with 29.5 million participants,"J. Am. Coll. Cardiol., vol. 71, p. A1819, 2018.

[3] M. A. Weber, F. Mahfoud, R. E. Schmieder, D. E. Kandzari, K. P. Tsioufis, R. R. Townsend, K. Kario, M. Böhm, A. S. P. Sharp, J. E. Davies, J. W. Osborn, G. D. Fink, D. E. Euler, D. L. Cohen, M. P. Schlaich, and M. D. Esler, "Renal denervation for treating hypertension: Current scientific and clinical evidence," JACC Cardiovasc. Interv., vol. 12, no. 12, pp. 1095-1105, 2019.

[4] D. L. Bhatt, D. E. Kandzari, W. W. O'Neill, R. D'Agostino, J. M. Flack, B. T. Katzen, M. B. Leon, M. Liu, L. Mauri, M. Negoita, S. A. Cohen, S. Oparil, K. Rocha-Singh, R. R. Townsend, and G. L. Bakris, "A controlled trial of renal denervation for resistant hypertension," N. Engl. J. Med., vol. 370, no. 15, pp. 1393-1401, 2014.

[5] M. Esler, "Renal denervation for treatment of drug-resistant hypertension," Trends in Cardiovascular Medicine, vol. 25, no. 2, pp. 107-115, 2015.

[6] D. E. Kandzari, D. L. Bhatt, S. Brar, C. M. Devireddy, M. Esler, M. Fahy, J. M. Flack, B. T. Katzen, J. Lea, D. P. Lee, M. B. Leon, A. Ma, J. Massaro, L. Mauri, S. Oparil, W. W. O'Neill, M. R. Patel, K. Rocha-Singh, P. A. Sobotka, L. Svetkey, R. R. Townsend, and G. L. Bakris, "Predictors of blood pressure response in the symplicity htn-3 trial," Eur. Heart J., vol. 36, no. 4, pp. 219-227, 2015.

[7] A. Rakhmadi, K. Saito, S. Matsuhara, T. Tajima, and N. Takeshita, "Comparison of Radio Frequency Current and Microwave Energy for Transcatheter Renal Denervation," IEEE J. Electromagn. RF Microw. Med. Biol., vol. 4, no. 2, pp. 89-96, 2020.

[8] C. Rossmann and D. Haemmerich, "Review of temperature dependence of thermal properties, dielectric properties, and perfusion of biological tissues at hyperthermic and ablation temperatures," Crit. Rev. Biomed. Eng., vol. 42, no. 6, pp. 467-492, 2014.

[9] L. Bianchi, F. Cavarzan, L. Ciampitti, M. Cremonesi, F. Grilli, and P. Saccomandi, "Thermophysical and mechanical properties of biological tissues as a function of temperature: A systematic literature review," Int. J. Hypertens., vol. 39, no. 1, pp. 297-340, 2022.

[10] Y. Endo, K. Saito and K. Ito, "Temperature analysis of liver tissue in microwave coagulation therapy considering tissue dehydration by heating," IEICE Trans. Electron., vol. E99-C, no. 2, pp. 257-265, 2016.

[11] H. Watanabe, Y. Kobayashi, M. Hashizume, and M. G. Fujie, "Modeling the temperature dependence of thermophysical properties: Study on the effect of temperature dependence for rfa," Annu. Int. Conf. IEEE Eng. Med. Biol. Soc., vol. 2009, pp. 5100-5105, 2009.

[12] A. Mohammadi, L. Bianchi, S. Korganbayev, M. De Landro, and P. Saccomandi, "Thermomechanical modeling of laser ablation therapy of tumors: Sensitivity analysis and optimization of influential variables," IEEE Trans. Biomed. Eng., vol. 69, no. 1, pp. 302-313, 2022.

[13] J. Choi, M. Morrissey, and J. C. Bischof, "Thermal processing of biological tissue at high temperatures: Impact of protein denaturation and water loss on the thermal properties of human and porcine liver in the range 25–80 °c," ASME. J. Heat Transfer., vol. 135, no. 6, 2013.

[14] S. R. Guntur, K. I. Lee, D. G. Paeng, A. J. Coleman, and M. J. Choi, "Temperature-dependent thermal properties of ¡i¿ex vivo¡/i¿ liver undergoing thermal ablation," Ultrasound Med. Biol., vol. 39, no. 10, pp. 1771-1784, 2013.

[15] N. P. Silva, A. Bottiglieri, R. C. Conceição, M. O'Halloran, and L. Farina, "Characterisation of ex vivo liver thermal properties for electromagnetic-based hyperthermic therapies," Sensors (Basel), vol. 20, no. 10, 2020.

[16] J. E. Fajardo, C. M. Carlevaro, F. Vericat, E. Berjano, and R. M. Irastorza, "Effect of the trabecular bone microstructure on measuring its thermal conductivity: A computer modeling-based study," J. Therm. Biol., vol. 77, pp. 131-136, 2018.

[17] N. C. Bhavaraju and J. W. Valvano, "Thermophysical properties of swine myocardium," Int. J. Thermophys., vol. 20, no. 2, pp. 665-676, 1999.

[18] A. Bhattacharya and R. L. Mahajan, "Temperature dependence of thermal conductivity of biological tissues," Physiol. Meas., vol. 24, no. 3, pp. 769-783, 2003.

[19] N. P. Silva, A. Bottiglieri, E. Porter, M. O'Halloran, and L. Farina, "Evaluation of thermal properties of ex vivo kidney up to ablative temperatures," in 8th European Medical and Biological Engineering Conference, eds. T. Jarm, A. Cvetkoska, S. Mahnič-Kalamiza, and D. Miklavcic, pp. 537-543, Springer International Publishing, Cham, 2021.

[20] S. A. Chernyadiev, V. B. Aretinsky, N. I. Sivkova, A. V. Zhilyakov, N. J. Korobova, V. I. Gorbatov, and M. Z. Faizullin, "A calorimetric study of baker's cyst biological tissues," Biophysics, vol. 63, no. 6, pp. 989-993, 2018.

[21] V. D'Ambrosio and F. Dughiero, "Numerical model for rf capacitive regional deep hyperthermia in pelvic tumors," Med. Biol. Eng. Comput., vol. 45, no. 5, pp. 459-466, 2007.

[22] R. Manago and K. Saito, "Coagulated region analysis in a microwave surgical device with temperature-dependent physical properties of tissue," IEICE Electron. Express, vol. 16, no. 9, pp. 20190131-20190131, 2019.

[23] F. Sano, T. Washio, and M. Matsumae, "Measurements of specific heat capacities required to build computer simulation models for laser thermotherapy of brain lesions," Tokai. J. Exp. Clin. Med., vol. 44, no. 4, pp. 80-84, 2019.

[24] D. M. Phinney, J. C. Frelka, and D. R. Heldman, "Composition-based prediction of temperature-dependent thermophysical food properties: Reevaluating component groups and prediction models," J. Food Sci., vol. 82, no. 1, pp. 6-15, 2017.

[25] T. Nagaoka, S. Watanabe, K. Sakurai, E. Kunieda, M. Taki, and Y. Yamanaka, "Development of realistic high-resolution whole-body voxel models of japanese adult males and females of average height and weight, and application of models to radio-frequency electromagnetic-field dosimetry," Phys. Med. Biol., vol. 49, no. 1, pp. 1-15, 2004.

[26] K. S. Yee, "Numerical Solution of Initial Boundary Value Problems Involving Maxwell's Equations in Isotropic Media," IEEE Trans. Antennas Propagat., vol. 14, no. 4, pp.302-207, 1966.

[27] H. H. Pennes, "Analysis of tissue and arterial blood temperatures in the resting human forearm. 1948," J. Appl. Physiol. (1985), vol. 85, no. 1, pp. 5-34, 1998.

[28] K. Saito, Y. Hayashi, H. Yoshimura, and K. Ito, "Heating characteristics of array applicator composed of two coaxial-slot antennas for microwave coagulation therapy," IEEE Trans. Microw. Theory Tech., vol. 48, no. 11, pp. 1800-1806, 2000.

[29] F. Fu, S. X. Xin, and W. Chen, "Temperature- and frequency-dependent dielectric properties of biological tissues within the temperature and frequency ranges typically used for magnetic resonance imaging-guided focused ultrasound surgery," Int. J. Hypertens., vol. 30, no. 1, pp. 56-65, 2014.

[30] C. W. Song, H. J. Park, C. K. Lee, and R. Griffin, "Implications of increased tumor blood flow and oxygenation caused by mild temperature hyperthermia in tumor treatment," Int. J. Hyperthermia, vol. 21, no. 8, pp. 761-767, 2005.
[31] Hasgall PA, Di Gennaro F, Baumgartner C, Neufeld E, Lloyd B, Gosselin MC, Payne D, Klingenböck A, Kuster N, "IT'IS Database for thermal and electromagnetic parameters of biological tissues," Version 4.1, 2022,.
[32] A. Rakhmadi and K. Saito, "Feasibility study of numerical calculation and machine learning hybrid approach for renal denervation temperature prediction," IEICE Trans. Electron., vol. E106-C, pp. 799-807, 2023.
[33] A. Rakhmadi, T. Hosoda, and K. Saito, "Microwave renal denervation temperature prediction using hybrid machine learning: *in silico* evaluation using human body model," IEICE Electron. Express, vol. 20, no. 11, pp. 20230118, 2023.

Tohgo Hosoda was born in Ibaraki, Japan, in 1999. He received an B.E. degree in medical engineering from Chiba University in 2019. He is working toward a M.E at the Graduate School of Science and Engineering, Chiba University, Chiba, Japan. His research interests in the area of medical applications of the electromagnetic fields and the machine learning of medical application.

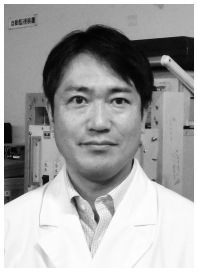

Kazuyuki Saito was born in Nagano, Japan, in 1973. He received the B.E., M.E., and D.E. degrees in electronic engineering from Chiba University, Chiba, Japan, in 1996, 1998 and 2001, respectively. He is currently an Associate Professor with the Center for Frontier Medical Engineering, Chiba University. His main interest is in the area of medical applications of the electromagnetic fields, including thermal treatment of cancer and microwave surgical devices etc. Dr. Saito is a senior member of the Institute of Electrical and Electronics Engineers (IEEE), the Institute of the Image Information and Television Engineers of Japan (ITE), the Japanese Society for Thermal Medicine (JSTM), and the Japan Society for Endoscopic Surgery (JSES). He received the IEICE AP-S Freshman Award, the Award for Young Scientist of URSI General Assembly, the IEEE AP-S Japan Chapter Young Engineer Award, the Young Researchers Award of IEICE, and the International Symposium on Antennas and Propagation (ISAP) Paper Award in 1997, 1999, 2000, 2004, and 2005 respectively.